PCCP

ROYAL SOCIETY OF CHEMISTRY

PAPER

View Article Online
View Journal | View Issue

Cite this: *Phys. Chem. Chem. Phys.*, 2025, **27**, 22954

On the mechanism of reactive sorption of H_2S on CuO (111) and ($\bar{1}$11) surfaces: a first-principles study

David Jiang,[a] Nicole Chiang,[a] Tirso López-Ausens[a] and Philippe Sautet *[ab]

Received 25th August 2025,
Accepted 6th October 2025

DOI: 10.1039/d5cp03246f

rsc.li/pccp

Hydrogen sulfide (H_2S) is a toxic and corrosive impurity present in industrial gas streams. An effective method for H_2S removal is through reactive sorption with metal oxides. This work investigates the reaction of H_2S on CuO surfaces to produce water and CuS. Using density functional theory (DFT), the elementary steps involved in H_2S adsorption and dissociation on the CuO (111) and ($\bar{1}$11) surfaces are modelled. The three-coordinated oxygen atoms (O_3c) on CuO surfaces are highly reactive and facilitate H_2S dissociation at room temperature, whereas four-coordinated oxygen atoms (O_4c) are less reactive, requiring higher temperatures for effective H_2S dissociation. Partial sulfidation of the surface, however, stabilizes the substitution of O_4c by sulfur, making the dissociation of H_2S thermodynamically favorable but kinetically demanding at room temperature. Proton transfer steps, such as water formation, are generally favorable, while heavier atom migrations (*e.g.*, hydroxyl migration and vacancy healing) are energetically costly. Near ambient temperature conditions promote the replacement of all O_3 and O_4 atoms at the surface, facilitating further sulfidation and H_2S adsorption. This computational understanding of the reaction mechanism provides insights into the reactive behavior of CuO surfaces in the purification of H_2S.

Introduction

Hydrogen sulfide (H_2S) contaminants in gas streams damage stream-carrying equipment and are environmentally hazardous.[1,2] Efficient removal of H_2S from fuel gas streams is crucial for profitable and safe gas conversion technologies.[3] One way to remove H_2S is through its reaction with a metal oxide to generate a metal sulfide and water. The approach involving the use of reactive sorption reactions is more efficient than trapping the molecule by physisorption in a porous compound since the thermodynamics of reactive sorption are more favorable. Among commercially regenerable metal oxides, ZnO, MnO, and CuO were found to be the most thermodynamically favorable for sulfur removal, but their usage has been mostly limited to temperatures above 250 °C due to kinetic limitations and the associated low utilization of the solid.[4–10] Operating at low temperatures can be more economical than at high temperatures, and crucial research efforts are devoted to design metal oxide materials that could perform sulfidation reactions at low temperatures and in particular, at room temperature.[5,11]

CuO has been considered a promising candidate due to the favorable sulfidation thermodynamics at ambient temperatures owing to its high equilibrium constant for sulfidation (K_s = 6.8 × 10^{20} at 298 K).[12] Previous work has focused on the synthesis of CuO nanoparticles to be either supported on mesoporous materials such as mesoporous silica (SBA-15)[13] or combined with other metal oxides. Baird *et al.* found that the Gibbs free energies of reaction (ΔG) for zinc oxide doped with CuO, ZnO, Fe_2O_3, and NiO were −126, −76, −74, and −136 kJ mol^{-1} respectively.[14] However, despite these favorable thermodynamics, H_2S uptake was quite low on all absorbents at 298 K.[14] Li *et al.* identified binary Cu–Cr–O and Cu–Ce–O oxides as capable of removing H_2S from fuel gas to less than 5–10 ppmv at temperatures ranging from 650 to 850 °C.[15] The sulfidation reaction of copper atoms dispersed in Cr_2O_3 and CeO_{2-x} was found to have low activation energies of 19.8 and 16.6 kJ mol^{-1} respectively.[15]

As the existing literature largely deals with supported or mixed oxide materials, there is a dearth of research into pure CuO at low temperatures. At ambient conditions, the process of H_2S decontamination is very challenging from a kinetic aspect. Indeed, experiments have shown that sulfidation of CuO particles at room temperature is limited by diffusion and

[a] *Chemical and Biomolecular Engineering Department, University of California Los Angeles, Los Angeles, CA 90095, USA. E-mail: sautet@ucla.edu*
[b] *Department of Chemistry and Biochemistry, University of California Los Angeles, Los Angeles, CA, 90095, USA*

demonstrates varying kinetic efficiencies across different samples.[11] To understand the low/varying efficiency of CuO sorbents, it is crucial to access a molecular scale view of the elementary reaction mechanism of H_2S interacting with various surfaces of CuO.

The dissociative adsorption of a single H_2S has been studied by density functional theory (DFT) on the CuO (111) surface,[16–19] which is the most stable CuO surface.[20] Azzam *et al.* studied the reaction of H_2S with CuO nanoparticles to form CuS in fixed-bed experiments.[21] Under reaction conditions of 294 K and 1 atm, the authors found that smaller CuO crystals had a higher sulfur removal capacity. The inverse relationship between crystallite size and H_2S removal performance held regardless of morphology, surface area, and pore structure of CuO nanoparticles. The ability of small nanoparticles to capture more H_2S suggests surface atoms are more reactive.[21] Additionally, the authors used DFT to identify that the 3-coodinated oxygens (O_{3C}), which are present to a greater extent on smaller nanoparticles, provide a better overall reaction energy towards H_2S compared to the 4-coodinated oxygens (O_{4C}), though without exploring the reaction mechanism.[21]

Further steps needed to form surface CuS and water have not been explored. On a more technical aspect, strong correlation effects at Cu have not been taken into account in these studies.[22,23] To our knowledge, no study has been done on the complete sulfidation mechanism of CuO surfaces. The literature suggests surface atoms are the dominant contributors to sulfidation of CuO[21] and this surface sulfidation process is modelled here using DFT calculations, while deeper sulfidation of the bulk is not considered. We report the mechanisms of the reactive sorption of H_2S on the CuO (111) and ($\bar{1}$11) surfaces to understand the elementary steps of initial surface sulfidation and compare the activity of the two most prominent surfaces of CuO particles. We show that the initial reactivity of CuO particles is occurring at the three-fold coordinated oxygen atoms on the surface, while reaction at the four-fold coordinated O atoms is initially thermodynamically unfavorable. Formation of water is thermodynamically and kinetically unfavorable at low H_2S coverage and room temperature conditions, such that OH groups stay on the surface until a high H_2S coverage is reached, at which point water desorption becomes possible. Once the low coordinated oxygen atoms are replaced by sulfur, exchange between sulfur and high coordinated oxygen becomes thermodynamically favorable, enabling further sulfidation of the surface.

Methods and models

Density functional theory (DFT) and atomistic thermodynamics were employed to construct reaction profiles by probing the potential energy surface (PES) at room temperature and ambient pressure. Specifically, DFT with a planewave basis set and the PBE exchange–correlation functional[24] with the Hubbard *U* correction were used with the VASP code.[25–28] A *U*-value of 7.0 eV was applied to Cu atoms to properly account for the strongly correlated, partially filled Cu 3d states. This *U*-value was chosen as it allows the model to correctly capture the experimentally observed bulk properties of CuO including magnetic moment and the band gap of CuO.[29] Other theoretical studies for the CuO(111) slab also employ the *U*-value of 7 eV for CuO to more accurately describe both the electronic structure and reaction energetics.[31]

The dDsC dispersion correction was used to describe long-range van der Waals interactions. The projector augmented-wave (PAW) method[32,33] was employed to describe the inner core–valence interaction with Cu having 11 valence electrons. The plane-wave basis set kinetic energy cutoff was set to 400 eV. The electronic energies and atomic forces were converged within 10^{-6} eV and 0.05 eV A^{-1} respectively. Gaussian smearing was employed with a width of 0.1 eV. The local minima on the potential energy hypersurface were found using the conjugate gradient method. The transition states utilized to find kinetic barriers were calculated *via* the climbing image-nudged elastic band (CI-NEB) method using eight images. The Gibbs free energy was calculated at a temperature of 298 K and a partial pressure for H_2S and H_2O of 101 Pa.

CuO shows a monoclinic crystal structure. From the Wulff construction, we know that the CuO nanoparticle surface is dominated by the CuO (111) and CuO ($\bar{1}$11) facets.[34] Of these two surfaces, the CuO (111) surface is more stable and has a surface free energy of 0.74 J m^{-2}, while CuO ($\bar{1}$11) surface has a surface free energy of 0.86 J m^{-2}.[23,34,35] Less stable than the (111) and ($\bar{1}$11) facets is the (011) facet with a surface free energy of 0.94 J m^{-2}.[34,35] Using these surface free energies to derive the Wulff crystal morphology[36] of CuO consisting of (111), ($\bar{1}$11), and (011), the polyhedron surface will consist of 38% of the (111) facet, 32% of the ($\bar{1}$11) facet, and 30% of the (011) facet. This study focuses on the similar (111) and ($\bar{1}$11) facets which dominate the Wulff morphology and make up a combined 70% of the CuO surface area. To model these CuO surfaces, we employ 2 × 1 slabs, presenting four O–Cu–O trilayers and 32 Cu and 32 O atoms in total (Fig. 1), using a 3 × 3 × 1 mesh to sample the Brillouin zone. Interactions between periodic images of adsorbates on neighboring unit cells have been tested and found to be negligible. For example, for the H_2S adsorbate a change from the 2 × 1 to the 2 × 2 unit cell leads to a variation of the Gibbs free adsorption energy of less than 0.03 eV. The two surfaces share the same two types of oxygen and copper atom, which are either three-fold or four-fold coordinated (O_{3c}, O_{4c}, Fig. 1). However, the four-fold oxygen (O_{4c}) is buried comparably lower into the subsurface on the CuO ($\bar{1}$11) surface (Fig. 1b). On the CuO (111) surface, O_{4c} is 0.3 Å below Cu_{4c} while on the CuO ($\bar{1}$11) surface this separation is 0.8 Å.

Results

Reaction mechanism for reactive sorption of a single H_2S

The mechanism was determined for the reactive sorption of a single H_2S molecule on CuO (111) and CuO ($\bar{1}$11) surfaces, where the stoichiometric reaction for the process is

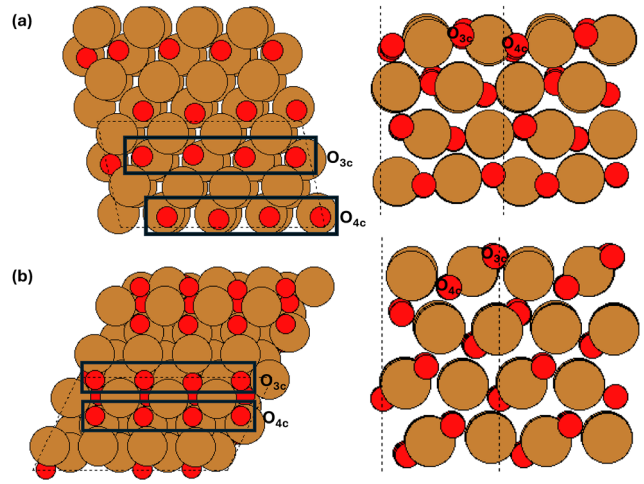

Fig. 1 Top (left) and side (right) view of the surface models for the (a) CuO (111) surface (b) CuO ($\bar{1}11$) surface considered in this study. Oxygen atoms are shown in red and copper atoms shown in brown. Dashed lines indicate unit cell boundaries. Black boxes indicate rows of three coordinated and four coordinated oxygens.

$$CuO + H_2S \rightarrow CuS + H_2O \quad (1)$$

Calculation results in Fig. 2. Show that the most favorable mechanism involves the following elementary steps (labels in parenthesis are used in Fig. 2 and 3):

1. Molecular adsorption of H_2S on the CuO surface (H_2S_a). Subscript "a" refers to a species "adsorbed" on top of the surface.

2. First S–H bond dissociation, producing SH and hydroxyl ad-species ($HS_a + O_lH$). Subscript "l" refers to an O atom in the "lattice" of the surface.

3. Second S–H bond dissociation, producing a sulfur adatom and a second hydroxyl ad-species ($S_a + 2O_lH$).

4. Activation of one hydroxyl by migration from its equilibrium position in the CuO lattice towards an adsorbed position on the surface, with formation of an oxygen vacancy ($S_a + O_lH + O_aH$). This step is key to make the path to water formation easier.

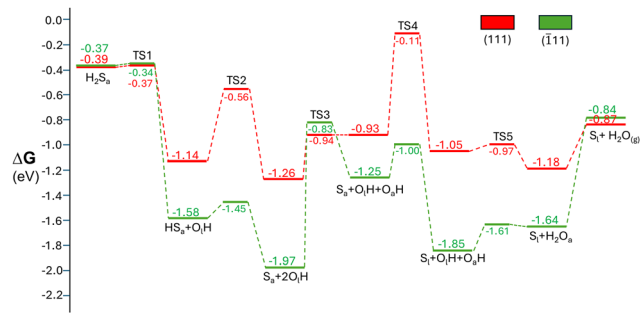

Fig. 2 Reaction profile showing the change in Gibbs free energy *versus* elementary reaction steps for reaction of a single H_2S molecule involving a three-coordinated O on bare CuO (111) surface in red and on bare CuO ($\bar{1}11$) surface in green. For free energy calculations, T = 298 K and P = 101 Pa. The free energy reference corresponds to that of the bare CuO and $H_2S_{(g)}$.

5. Healing of previously created oxygen vacancy by the sulfur atom, which becomes a "lattice" sulfur ($S_l + O_lH + O_aH$).

6. Formation of water by proton transfer from one hydroxyl to another hydroxyl group ($S_l + H_2O_a$; formed lattice O is not explicitly indicated).

7. Eventually, desorption of water ($S_l + H_2O_{(g)}$ where (g) indicates a gas phase species).

The reaction mechanism depends strongly on whether O_{3c} or O_{4c} atoms are considered. The Gibbs free energy pathways for H_2S adsorption and reaction with O_3c on (111) and ($\bar{1}11$) facets are shown in Fig. 2, while structures for intermediates are given in Fig. 3. A Sideview of each intermediate is provided in Fig. S1. For each step, the Cu atom producing the most favorable energy is selected, either Cu_{3c} or Cu_{4c}. We observe on Fig. 2 that the exchange between O_{3c} and sulfur is thermodynamically favorable relative to gas phase H_2S, by −0.87 eV and −0.84 eV on the (111) and ($\bar{1}11$) surfaces respectively. H_2S is chemisorbed on the surface with an optimal position for the S atom 2.6 Å atop a Cu_{3c} atom. The chemisorption is exergonic on both CuO (111) and CuO ($\bar{1}11$) surfaces. The first S–H dissociation occurs with a low barrier. For the CuO ($\bar{1}11$) surface, this barrier is +0.03 eV and for the CuO (111) surface it is +0.02 eV. These can be very quickly passed at room temperature. The created SH fragment preferentially sits on a bridge site formed by two Cu_{3c} atoms. This first S–H bond dissociation is highly exergonic (by −0.75 and −1.21 eV with respect to adsorbed H_2S on the (111) and ($\bar{1}11$) surfaces respectively). The second S–H dissociation is accordingly less exergonic relative to the first but still proceeds with reasonably low energy barriers passable at room temperature (highest barrier is +0.58 eV on CuO (111)).

Once H_2S is transformed into S and two OH groups on the surface, the next steps are vacancy formation, migration of S into a lattice position, and water formation. The path for water formation will first be described and alternative pathways presented in the following sections. A key insight from DFT is that direct water formation is unfavorable and surface displacement of one OH from its lattice site to an adsorbed site on the surface is first needed. This displacement of one hydroxyl group is energetically uphill by +0.33 eV on the CuO (111) surface and +0.72 eV on the CuO ($\bar{1}11$) surface but opens the way for the migration of the S atom into the freed lattice site. The barrier to displace a hydroxyl (energy difference between $S_a + 2O_lH$ and TS3) is very different on the two surfaces, +1.14 eV and +0.32 eV on ($\bar{1}11$) and (111) respectively. The barrier for CuO ($\bar{1}11$) cannot be passed at room temperature. The reaction would hence be blocked at the $S_a + 2O_lH$ intermediate due to unfavorable thermodynamics for both facets as the Gibbs free energy of all following intermediates is higher. The CuO ($\bar{1}11$) would also be hindered at this intermediate due to high kinetic barriers.

The vacancy healing by the S atom represents another major difference between the two systems. While the movement of sulfur for vacancy healing is facile on CuO ($\bar{1}11$), a simultaneous activated movement of the hydroxyl group is required on CuO (111): costly because the hydroxyl group goes through a

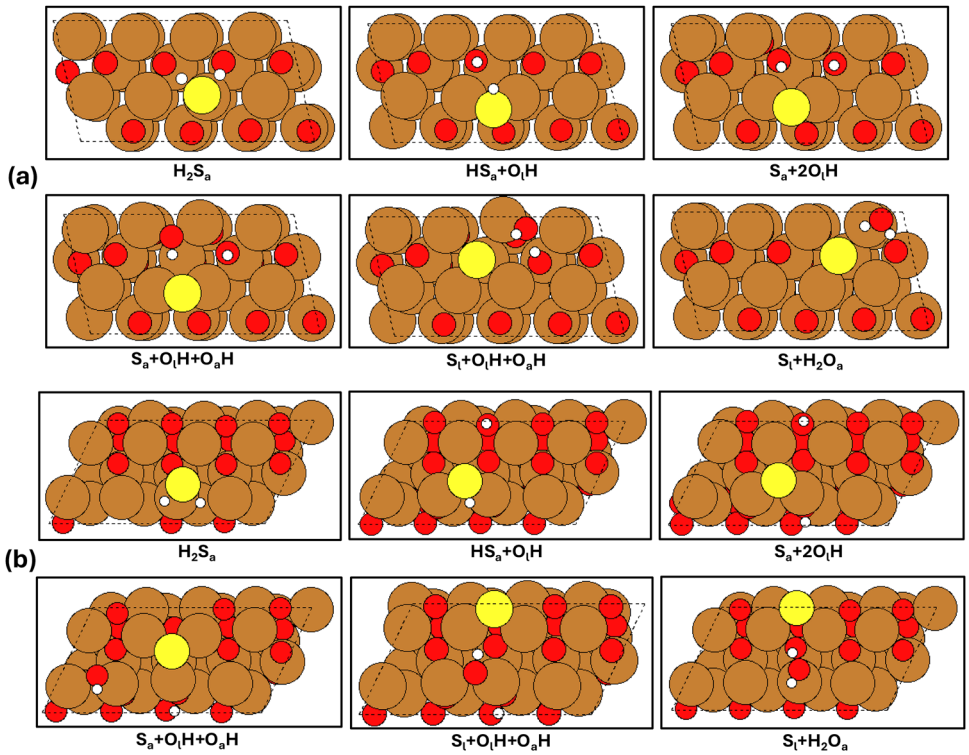

Fig. 3 Structures for reaction intermediates involving (a) O_{3c} with a single H_2S molecule on bare CuO (111) surface (b) and O_{3c} with a single H_2S molecule on bare CuO ($\bar{1}11$) surface. Oxygen atoms are shown in red and copper atoms in brown and sulfur atoms in yellow.

change of coordination from two to one copper atom (Fig. 4a). For CuO (111) the most stable configuration with the activated hydroxyl is one in which the hydroxyl is activated onto a copper bridge site closest to the original equilibrium position (Fig. 4a, left structure). The close proximity puts the hydroxyl group hovering halfway above the vacancy site near the sulfur, such that there is a favorable interaction between the hydrogen of the hydroxyl and the sulfur atom (distance 2.0 Å). This stabilizing effect plays a role in minimizing the energy cost of migrating the hydroxyl group. In the next vacancy healing step, the hydroxyl group is pushed to the side to fully expose the vacancy, allowing sulfur to take its place (Fig. 4a, TS4 and right structure). The coupled movement of the sulfur and the hydroxyl group causes a change of hydroxyl group environment that explains the higher transition state barrier on CuO (111). For the ($\bar{1}11$) surface as shown in Fig. 4b, the OH group in its bridge site is further away from the S atom and can remain in this site during the migration of the S atom.

The energetics of sulfidation by reactive sorption of H_2S, involving the substitution of one O atom by a S atom, on the

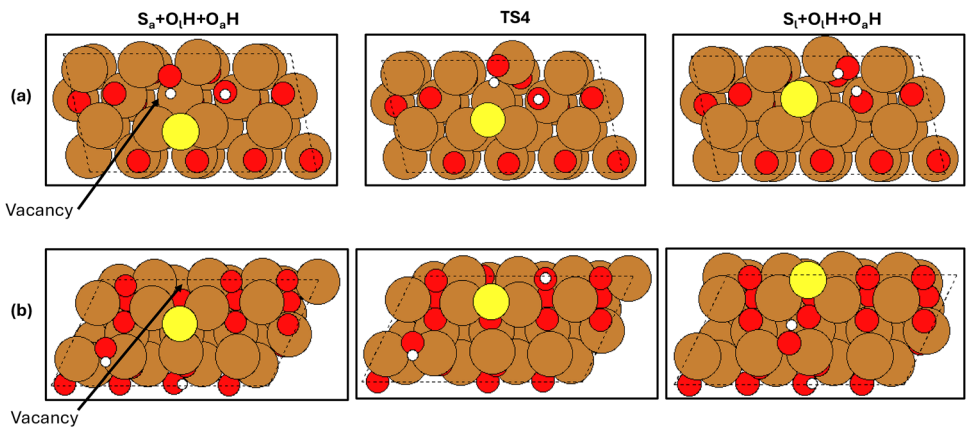

Fig. 4 Structures of transition states (TS4 in Fig. 2) and corresponding initial and final elementary step structures for the healing of the oxygen vacancy by the surface S atom, comparing O_{3c} pathways on (a) the CuO (111) surface and on the (b) the CuO ($\bar{1}11$) surface. A change in the hydroxyl coordination to Cu is required on the CuO (111) surface to expose the vacancy to S.

CuO ($\bar{1}11$) and CuO (111) surfaces can be compared with the equivalent reaction in the bulk of CuO. Sulfidation of bulk CuO with a low S content of 25% (exchange of one O atom among four O atoms), while maintaining the monoclinic structure of CuO, shows a calculated reaction Gibbs free energy of +0.12 eV. The reaction in bulk is endergonic and much less favorable compared to the −0.84 eV and −0.87 eV for the exergonic sulfidation on the CuO ($\bar{1}11$) and CuO (111) surfaces respectively. Therefore, initial sulfidation of the surface is favorable, while the initial sulfidation of the bulk is unfavorable. This contrasts with the total sulfidation of CuO bulk, with change of the crystal structure to the hexagonal system, which is well known to be exergonic. The standard enthalpy of reaction according to experimental standard enthalpies of formation[37–39] is −1.23 eV, while the standard reaction enthalpy from the DFT calculations is −1.29 eV, which is in very good agreement with the experimental value. The standard Gibbs free energy of formation was calculated to be −1.45 eV.

From the kinetic study on the CuO surfaces, the rate limiting step for CuO ($\bar{1}11$) is the formation of the vacancy by migration of an OH onto the surface with an effective barrier of +1.14 eV. The rate limiting step for CuO (111) is the migration of the S atom to the lattice site. The effective barrier for the (111) surface is +1.15 eV. Kinetically, the two systems show significant similarities. Comparing the two facets, the CuO ($\bar{1}11$) surface is more reactive, as seen from the energy profile in Fig. 2 where H_2S dissociation is more exergonic. Therefore, ($\bar{1}11$) will be investigated in more detail in the following sections.

Low reactivity of four-coordinated oxygen atoms (O_{4c})

Compared to O_{3c}, O_{4c} has a lower reactivity, to the extent that eqn (1) is no longer thermodynamically favorable for a single H_2S molecule forming surface S (at the O_{4c} site) and gaseous water (Fig. 5). The exchange between O_{4c} and sulfur is thermodynamically uphill relative to gas phase H_2S. This is consistent with the results shown by Azzam *et al.* who also identified O_{3C} as being more reactive.[21] The calculations show a Gibbs free energy of reaction of +0.56 eV for O_{4c} on the CuO ($\bar{1}11$) surface. The lower reactivity of O_4c on CuO ($\bar{1}11$) can be explained by the positions of the oxygens as O_{4c} is buried deeper in the subsurface. H_2S is initially chemisorbed on the surface, 2.6 Å atop a Cu_{3c} atom. The first HS bond dissociation on O_4c is exergonic (ΔG = −0.14 eV) while the second is endergonic (ΔG = 0.51 eV). This stands in contrast to the highly exergonic first and second HS bond dissociation (ΔG = −1.21 eV and −0.39 eV respectively) observed for H_2S deprotonation towards O_{3c} atoms for ($\bar{1}11$) in Fig. 5. Despite the need for small distortions of the surface copper atoms needed to accommodate the large sulfur atom, the complete healing of the vacancy is exergonic for both O_{4C} and O_{3C} with (ΔG = −0.12 and −0.6 eV respectively). For the O_{4C} pathway, just like for O_{3c} atoms, water formation on the surface is endergonic (ΔG = 0.48 eV).

The difference in reactivity of O_3c and O_4c atoms for sulfur substitution can be related to the cost of O vacancy formation. For CuO ($\bar{1}11$), the oxygen vacancy formation free energies were found to be +2.73 eV and +3.27 eV for O_{3C} and O_{4c} respectively by applying the correction for the O_2 binding energy when using GGA exchange correlation functionals proposed by Wang *et al.*[30] Therefore, the smaller cost of vacancy formation correlates with the reactivity. Prior work by Maimaiti *et al.* using the hybrid HSE06 functional show a similar trend for the oxygen vacancy formation energy on CuO (111) with +2.77 eV for the O_{3C} and +3.27 for O_{4c}.[31]

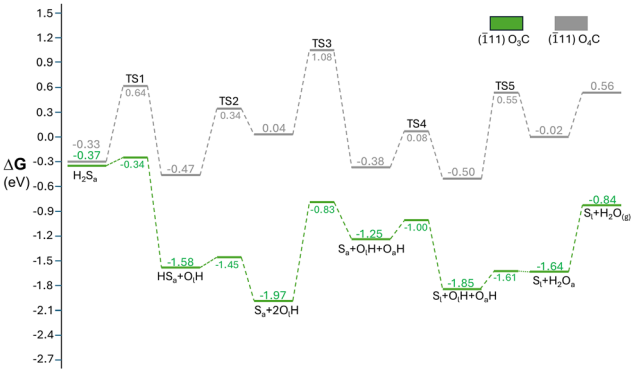

Fig. 5 Reaction profile showing change in Gibbs free energy *versus* elementary reaction steps for reactions involving O_{3c} with a single H_2S molecule on the bare CuO ($\bar{1}11$) surface in green and O_{4c} with a single H_2S molecule on the bare CuO ($\bar{1}11$) surface in gray. For the free energy calculations, T = 298 K and P = 101 Pa.

Reaction of H_2S on O_{4c} oxygen atoms also results in much higher energy barriers (Fig. 5). Steps involving transfer of hydrogen atoms show barriers in the range of +0.75 to +1.0 eV. Water formation barrier for the O_{4c} pathway is about 1.0 eV. The origin of the higher barriers lies in the location of the O_{4c} atoms within the subsurface. Hydrogen transfer between adspecies on the surface and species in the subsurface encounters two difficulties: one is hindrance from the surface copper atoms and the second is longer distances between initial and final states of the hydrogen atom that result in less stable transition states. The highest transition state along the pathway corresponds to the rearrangement of S and OH required for water formation (TS3), linked with an effective activation energy of 1.55 eV, a barrier not overcome at a significant rate at room temperature. Hence, transformation of the O_{4c} atoms near the surface is both thermodynamically and kinetically limited for the surface sulfidation of CuO, in contrast with O_{3c}. This suggests that when the reaction begins, initial sulfidation occurs as a result of exchange between sulfur atoms and O_{3c}. The initial sulfidation would transform the surface into a partially sulfided surface.

The reaction pathway at O_3c atoms indicates that water formation on the surface is endergonic if a single H_2S molecule reacts. The activation barriers associated with this reaction are high. In the next section, a high coverage of OH groups resulting from the dissociation of several H_2S molecules is explored. Elevated coverage enables water formation to be thermodynamically favorable and greatly lowers the associated kinetic barriers.

Adsorption and reaction at high S coverage

The previous study of the reaction of a single H_2S molecule invites, after the dissociation of that first H_2S molecule (to form the S_a + $2O_lH$ intermediate), continued adsorption and dissociation of additional H_2S molecules to study a reaction mechanism at a higher S coverage. Selecting the CuO ($\bar{1}11$) surface due to its more favorable thermodynamics, the addition of two additional H_2S molecules starting from the previously described free energy well of S_a + $2O_lH$ was modelled.

At higher H_2S coverage, formation of adsorbed water becomes overall exergonic. The two H_2S molecules are first chemisorbed 2.8 Å and 2.6 Å atop Cu_{3c} atoms (S_a + $2O_lH$ + $2H_2S_a$ on Fig. 6 and 7). At this point, favorable Cu_{3c} adsorption sites in the unit cell are fully occupied. One H_2S transfers both of its protons to two O_{3c} atoms. At this intermediate ($2S_a$ + $4O_lH$ + H_2S_a on Fig. 6 and 7), all surface O_{3c} are protonated to form hydroxyls. The produced sulfur atom forms a disulfide bond with the first surface sulfur. Formation of disulfide bonds is exergonic and such bonds are seen in the CuS solid.

The following step (forming $2S_a$ + $3O_lH$ + H_2S_a + O_aH on Fig. 6 and 7) is hydroxyl migration and at such a high OH coverage is only uphill by +0.15 eV (instead of +0.72 eV on Fig. 2). Indeed, hydroxyl migration is stabilized by two hydrogen bonds, one between the hydroxyl and the polysulfide species at a H–S distance of 2.1 Å and another between hydroxyl and H_2S at a H–O distance of 2.3 Å (Fig. 8a). The weakly endergonic character of OH migration is key since it allows the OH to move close to the third chemisorbed H_2S molecule. Water formation can occur by a proton transfer from that neighboring H_2S rather than from another OH. Such a step is markedly exergonic. The formed H_2O is displaced from its initial "lattice" site and replaced by S, forming the first "lattice" surface S atom. The final step of water formation is favorable due to the abundance of adspecies on the surface, including the SH group formed by the dissociation of the third H_2S molecule (Fig. 8c). Hence at high coverage, specific lateral interactions (disulfide bond formation, hydrogen bonding) make hydroxyl migration and water formation facile.

If the adsorption step is excluded, elementary steps for this mechanism can be classified into two different types. The first is a proton hopping process. This is the case for the first and second S–H bond activation and the water formation. The second type corresponds to migration of heavier atoms. This is the case for migration of hydroxyl group from the lattice position and healing of an oxygen vacancy by a sulfur atom. Proton hopping steps are generally thermodynamically and kinetically favorable as long as O_{3c} sites are available, the first one of these (S–H bond cleavage from H_2S) being more exergonic than the second (from S–H to S). Water formation *via* proton transfer from one hydroxyl to another is also generally easy.

The thermodynamic bottlenecks and kinetic limiting steps are the migrations of heavier atoms: migration of hydroxyl species from the lattice position can be energetically costly at low coverage but becomes easier at high coverage since stabilizing H-bond interactions can occur. On the other hand, the healing of an oxygen vacancy by a sulfur atom is quite favorable. This is expected, as oxygen vacancies are unstable on CuO surfaces.[31]

With a higher coverage of H_2S molecules, the path to formation of H_2O becomes achievable at ambient conditions. The desorption of water, endergonic by +0.54 eV at room temperature can be facilitated by further adsorption of H_2S molecules which will continue to react, resulting in the substitution of additional lattice O atoms by S atoms. As shown in Fig. 5, the O_{3C} atoms are more active than the O_{4C}, therefore the lower coordination oxygens will first be replaced by sulfur atoms, leading to a saturated surface in which all O_{3C} atoms have been substituted by sulfur.

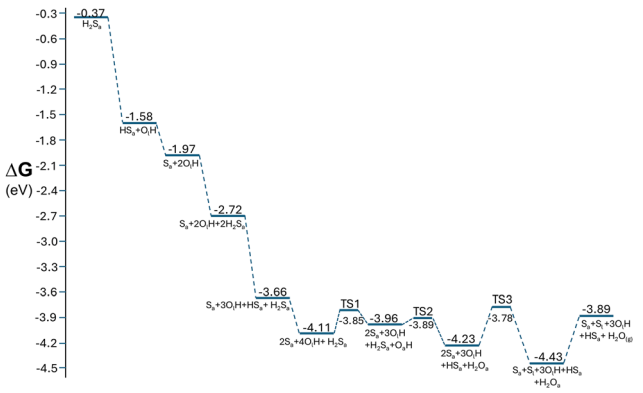

Fig. 6 Reaction profile showing the change in Gibbs free energy *versus* elementary reaction steps for reaction of three H_2S molecules on the CuO ($\bar{1}11$) surface. After the second deprotonation of the first H_2S molecule (S_a + $2O_lH$), a second and third H_2S are added simultaneously and reacted until the formation of a single H_2O molecule. Corresponding structures are shown in Fig. 7. For the free energy calculation, T = 298 K and P = 101 Pa.

Effect of extent of surface sulfidation

The unfavorable reaction at the four-coordinated O atoms on the surface is an impediment to H_2S decontamination. However, after extensive sulfidation of the surface at the reactive three-coordinated oxygens, the situation changes such that reaction at O_{4c} can be facilitated. A partially sulfided model was constructed where each surface O_{3c} atom has been substituted by a S atom starting from the CuO ($\bar{1}11$) surface (Fig. 9). In this model, only four-coordinated O atoms are available for further reaction.

Sulfidation of the surface is associated with shifts in surface charge distribution. The bonds between Cu and O atoms on pristine CuO ($\bar{1}11$) (Fig. 1b) are more ionic than the bonds between Cu and S on the partially sulfided surface (Fig. 9). The Bader charge of the O_{3c} on pristine CuO is −0.95 and the average Bader charge of the surface Cu atoms is +0.98. On the partially sulfided system (Fig. 9), the Bader charge of the S_{3c} is −0.33 and the average Bader charge of the surface Cu atoms is +0.63. Though the formal oxidation number of Cu does not change when oxygen is substituted by sulfur through repeated H_2S reactions, the charge of Cu is reduced as the Cu–S bonds

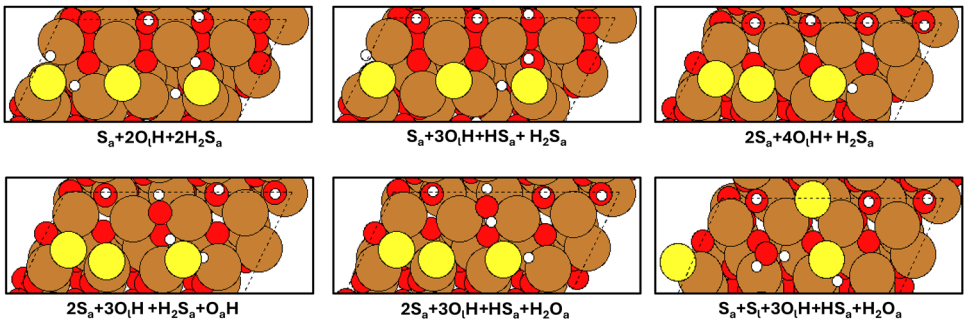

Fig. 7 Stable structures along the reaction pathway of Fig. 6 involving the addition of a second and third H_2S to the O_{3c} ($\bar{1}11$) pathway after the second deprotonation of the first H_2S and reaction until the formation of a single H_2O molecule.

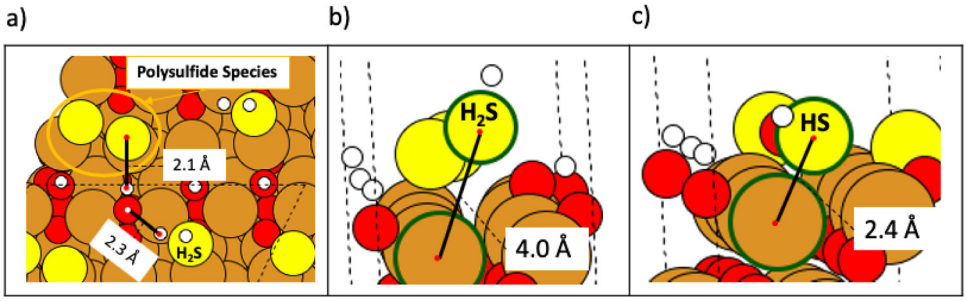

Fig. 8 Structures of (a) OH migration top view showing stabilizing interactions (b) OH migration side view showing H_2S physisorption and (c) water formation showing HS chemisorption on the surface for the reaction involving addition of 2 H_2S to the O_{3c} ($\bar{1}11$) pathway.

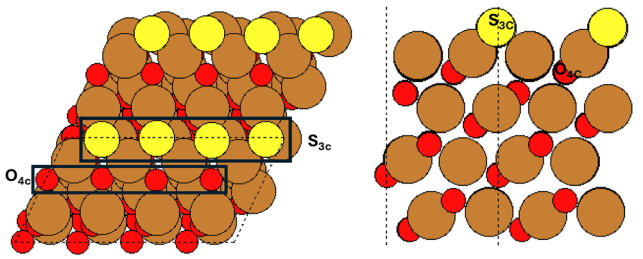

Fig. 9 Top and side view of surface models for partially sulfided CuO ($\bar{1}11$) surface. Each S_{3c} is a three-coordinated sulfur atom occupying the lattice sites initially occupied by a O_{3c} surface atom.

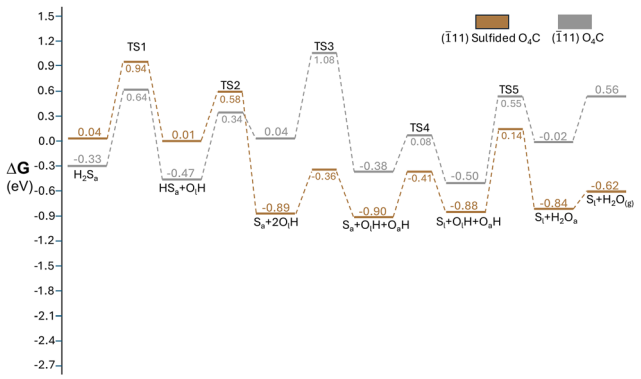

Fig. 10 Reaction profile showing change in Gibbs free energy *versus* elementary reaction steps for O_{4c} with a single H_2S molecule on partially sulfided CuO ($\bar{1}11$) surface in brown and O_{4c} with a single H_2S molecule on bare CuO ($\bar{1}11$) surface in gray. For the free energy calculation, T = 298 K and P = 101 Pa.

are more covalent in nature than the Cu–O bonds due to weaker electronegativity of sulfur compared to oxygen.

On the partially sulfided ($\bar{1}11$) surface, we found that the exchange of the remaining O_{4c} with sulfur becomes favorable thermodynamically, with an overall Gibbs free energy of reaction of −0.62 eV relative to gas phase H_2S. (Fig. 10). The intermediates and reaction mechanism for O_{4c} are shown on Fig. 11. Sideview of each intermediate is provided in Fig. S6.

The initial adsorption of H_2S is weak on the partially sulfided surface, with a Gibbs free adsorption energy close to zero (H_2S_a in Fig. 10, ΔG = +0.04 eV). The two S–H bond dissociation steps are exergonic, with the second dissociation (ΔG = −0.90 eV) much more exergonic than the first (ΔG = −0.03 eV). The reaction energy for S–H bond dissociation is, however, less strong than that observed for O_{3c} atoms on the bare ($\bar{1}11$) surface, implying that while sulfidation of the surface improves the reactivity of O_{4c}, the change is not enough to match the higher reactivity of O_{3c} atoms. The sulfur produced by H_2S dissociation forms a disulfide species with a surface sulfur atom at a bond distance of 2.0 Å, which is a factor of stability for the intermediates, such as $S_a + O_lH + O_aH$, shown in

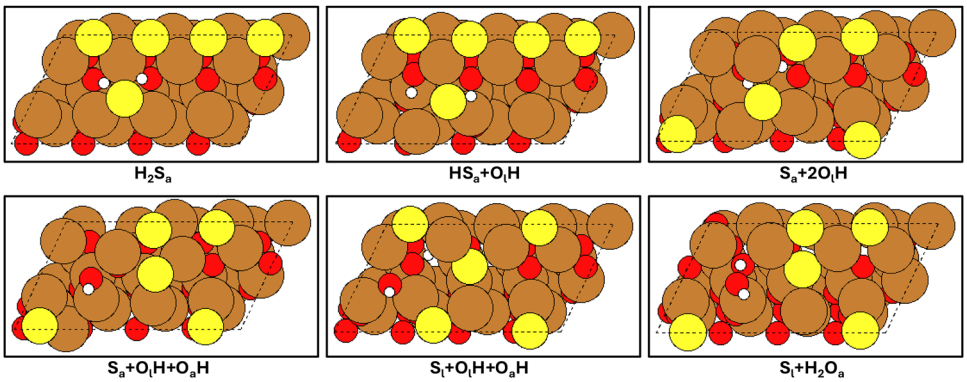

Fig. 11 Stable structures along the reaction pathway of Fig. 10 for reaction of O_{4c} on the partially sulfided CuO ($\bar{1}11$) surface.

Fig. 11. The thermodynamics of the reaction are thus improved. Water formation and desorption, *i.e.* from S_a + O_lH + O_aH to (S_l + $H_2O_{(g)}$), is only slightly endergonic (+ 0.28 eV), however the barrier of +1.04 is significant (effective barrier from S_a + O_lH + O_aH to TS5). Altogether, the largest elementary barrier for the reaction of H_2S on remaining O_{4c} after all O_{3c} are replaced by sulfur is associated with the water formation (+1.02 eV) as shown on Fig. 10. However, prior results demonstrate that a higher coverage is important to facilitate water formation and the same coverage effects should also be present on the partially sulfided surface.

Conclusions

The reactive sorption of H_2S over CuO (111) and ($\bar{1}11$) surfaces has been investigated from a computational vantage to shed light on the dissociation mechanism at the atomic level, elucidating the elementary steps that comprise the reaction mechanism.

The main reaction mechanism studied begins with molecular adsorption of H_2S on the surface, followed by a S–H bond dissociation resulting in SH and OH. The second S–H dissociation results in a S atom and hydroxyl groups. Then, one hydroxyl group migrates from the lattice position creating an oxygen vacancy, which is subsequently healed by the sulfur atom. Following that, a water molecule is formed *via* a proton transfer from one hydroxyl group to the other. The final step is water desorption from the surface.

Our calculations show that three-coordinated O atoms at the surface of CuO can be easily hydroxylated upon H_2S dissociation, making this step possible at room temperature. However, water formation from OH groups at low coverage was found to be thermodynamically and kinetically challenging, such that additional H_2S molecules will dissociatively adsorb until a high OH coverage is reached, wherein water formation becomes feasible. In contrast to the O_{3c}, four-coordinated O atoms that are placed deeper in the surface are less active and cannot initially react at room temperature, largely due to the unfavorable thermodynamics of sulfur substitution.

The situation changes when all O_{3c} have been replaced by sulfur. The partial sulfidation of the surface stabilizes the substitution at the O_{4c}, presumably from strain and electronic effects exerted by the sulfide surface species. The reaction at O_{4c} becomes thermodynamically possible. However, with a barrier of +0.90 eV for H_2S dissociation, there would be a slow reaction rate at room temperature and slightly elevated temperatures around 353 K would be required. A further barrier also occurs for water formation, but such a barrier should be reduced at high OH coverage as seen for the reaction at O_{3c}. Altogether, all surface O_3 and subsurface O_4 atoms should be replaced at near ambient temperatures. This facile sulfidation at the surface of particles qualitatively agrees with experiments that show a high sulfidation efficiency on small CuO particles.[11,21]

The elementary steps in the reaction can be organized into two different types of steps according to their nature: proton hopping processes in which one proton is transferred from one group to another and migration of heavier groups between the lattice and the surface. Proton hopping is found to be relatively easy while migrations of heavier atoms, such as hydroxyl species, is energetically costly in most cases.

After the surface has been sulfided, further growth of the sulfide requires reaction of sulfur atoms within the lower subsurface region, which is not directly feasible. It first requires vacancy mediated migration of subsurface O atoms towards the surface region and migration of S towards the subsurface, hence enriching the surface region in O atoms for further reaction. It also requires the nucleation of CuS domains with their different crystal structure, since the substitution of O atoms by S atoms in the CuO bulk crystal structure is not thermodynamically favorable.

Conflicts of interest

There are no conflicts to declare.

Data availability

The data supporting this article have been included as part of the supplementary information (SI). Supplementary information: calculated transition state (TS) structures for all decomposition reaction pathways and surface models of H_2S adsorbed

on CuO (111) and ($\bar{1}$11). See DOI: https://doi.org/10.1039/d5cp03246f.

Acknowledgements

DJ and PS acknowledge support from the U.S. Army Research Laboratory and the U.S. Army Research Office under Grant No. W911NF-21-1-0361. Computations in this work were performed on the Expanse Supercomputer and on the Bridges2 cluster through allocation CHE170060 from the Advanced Cyberinfrastructure Coordination Ecosystem: Services & Support (ACCESS) supported by the National Science Foundation.

References

1 M. J. Goodwin, O. M. Musa and J. W. Steed, Problems Associated with Sour Gas in the Oilfield Industry and Their Solutions, *Energy Fuels*, 2015, **29**, 4667–4682.
2 R. O. Beauchamp, J. S. Bus, J. A. Popp, C. J. Boreiko, D. A. Andjelkovich and P. Leber, A Critical Review of the Literature on Hydrogen Sulfide Toxicity, *Crit. Rev. Toxicol.*, 1984, **13**, 25–97.
3 S. Rasi, J. Läntelä and J. Rintala, Trace Compounds Affecting Biogas Energy Utilisation—A Review, *Energy Convers. Manag.*, 2011, **52**(12), 3369–3375.
4 M. D. Dolan, A. Y. Ilyushechkin, K. G. Mclennan and S. D. Sharma, Sulfur Removal from Coal-Derived Syngas: Thermodynamic Considerations and Review, *Asia-Pac. J. of Chem. Eng.*, 2010, **7**, 1–13.
5 M. Balsamo, S. Cimino, G. D. Falco, A. Erto and L. Lisi, ZnO-CuO Supported on Activated Carbon for H2S Removal at Room Temperature, *Chem. Eng. J.*, 2016, **304**, 399–407.
6 J. Abbasian and R. B. Slimane, A Regenerable Copper-Based Sorbent for H2S Removal from Coal Gases, *Ind. Eng. Chem. Res.*, 1998, **37**, 2775–2782.
7 R. Sadegh-Vaziri and M. U. Babler, Removal of Hydrogen Sulfide with Metal Oxides in Packed Bed Reactors—A Review from a Modeling Perspective with Practical Implications, *Appl. Sci.*, 2019, **9**, 5316.
8 L. D. Gasper-Galvin, A. T. Atimtay and R. P. Gupta, Zeolite-Supported Metal Oxide Sorbents for Hot-Gas Desulfurization, *Ind. Eng. Chem. Res.*, 1998, **37**, 4157–4166.
9 V. Jalan, *Studies Involving High Temperature Desulfurization/Regeneration Reactions of Metal Oxides for Fuel Cell Development. Final report (No. DOE/MC/16021-1486). NTIS/DE84003096*, U.S. Department of Energy, Washington, DC, 1983, 17–19.
10 S. Kumar, R. Chaurasiya, M. A. Khan, G. Meng, J. S. Chen and M. Kumar, Enhancement of H2S Sensing Performance of rGO Decorated CuO Thin Films: Experimental and DFT Studies, *J. Phys.: Condens. Matter*, 2022, **35**(6), 064001.
11 A. S. Hoffman, S. Azzam, K. Zhang, Y. Xu, Y. Liu, S. R. Bare and D. A. Simonetti, Direct Observation of the Kinetics of Gas–Solid Reactions using In Situ Kinetic and Spectroscopic Techniques. React, *Chem. Eng.*, 2018, **3**, 668–675.
12 O. Knacke; O. Kubaschewski and K. Hesselmann, *Thermochemical properties of inorganic substances*, 1991.
13 O. Karvan and H. Atakül, Investigation of CuO/mesoporous SBA-15 sorbents for hot gas desulfurization, *Fuel Process. Technol.*, 2008, **89**, 908–915.
14 T. Baird, P. J. Denny, R. Hoyle, F. McMonagle, D. Stirling and J. Tweedy, Modified zinc oxide absorbents for low-temperature gas desulfurisation, *J. Chem. Soc. Faraday Trans.*, 1992, **88**, 3375–3382.
15 Z. Li and M. Flytzani-Stephanopoulos, Cu–Cr–O and Cu–Ce–O Regenerable Oxide Sorbents for Hot Gas Desulfurization, *Ind. Eng. Chem. Res.*, 1997, **36**, 187–196.
16 J. Zhang, M. Liu, R. Zhang, B. Wang and Z. Huang, Insight into the Properties of Stoichiometric, Reduced and Sulfurized CuO Surfaces: Structure Sensitivity for H2S Adsorption and Dissociation, *Mol. Catal.*, 2017, **438**, 130–142.
17 S. Sun, Y. Wang and Q. Yang, Density Functional Theory Study of the Methanol Adsorption and Dissociation on CuO (111) Surface, *Appl. Surf. Sci.*, 2014, **313**, 777–783.
18 S. Sun, D. Zhang, C. Li and Y. Wang, DFT Study on the Adsorption and Dissociation of H2S on CuO (111) Surface, *RSC Adv.*, 2015, **5**(28), 21806–21811.
19 C. Zheng and H. Zhao, Exploring the Microscopic Reaction Mechanism of H2S and COS with CuO Oxygen Carrier in Chemical Looping Combustion, *Fuel Process. Technol.*, 2020, **205**, 106431.
20 N. Y. Dzade, A. Roldan and N. H. D. Leeuw, Activation and Dissociation of CO_2 on the (001), (011), and (111) Surfaces of Mackinawite (FeS): A Dispersion-Corrected DFT Study, *J. Chem. Phys.*, 2015, **143**, 094703.
21 S. A. Azzam, F. H. Alshafei, T. Lopez-Ausens, R. Ghosh, A. N. Biswas, P. Sautet, S. Prikhodko and D. A. Simonetti, Effects of morphology and surface properties of copper oxide on the removal of hydrogen sulfide from gaseous streams, *Ind. Eng. Chem. Res.*, 2019, **58**, 18836–18847.
22 A. J. Cohen, P. Mori-Sánchez and W. Yang, Challenges for Density Functional Theory, *Chem. Rev.*, 2012, **112**, 289–320.
23 S. L. Dudarev, G. A. Botton, S. Y. Savrasov, C. J. Humphreys and A. P. Sutton, Electron-Energy-Loss Spectra and the Structural Stability of Nickel Oxide: An LSDA U Study, *Phys. Rev. B: Condens. Matter Mater. Phys.*, 1998, **57**, 1505–1509.
24 J. P. Perdew, K. Burke and M. Ernzerhof, Generalized Gradient Approximation Made simple, *Phys. Rev. Lett.*, 1996, **77**(18), 3865.
25 G. Kresse and J. Furthmüller, Efficiency of Ab-Initio Total Energy Calculations for Metals and Semiconductors Using a Plane-Wave Basis Set, *J. Comput. Mater. Sci.*, 1996, **6**(1), 15–50.
26 G. Kresse and J. Furthmüller, Efficient Iterative Schemes for Ab Initio Total-Energy Calculations Using a Plane-Wave Basis Set, *Phys. Rev. B: Condens. Matter Mater. Phys.*, 1996, **54**(16), 11169.
27 G. Kresse and J. Hafner, Ab Initio Molecular-Dynamics Simulation of the Liquid-Metal–Amorphous-Semiconductor Transition in Germanium, *Phys. Rev. B: Condens. Matter Mater. Phys.*, 1994, **49**(20), 14251.
28 G. Kresse and J. Hafner, Ab initio Molecular Dynamics for Liquid Metals, *Phys. Rev. B: Condens. Matter Mater. Phys.*, 1993, **47**(1), 558.

29 M. Nolan and S. D. Elliott, The P-Type Conduction Mechanism in Cu2O: a first principles study, *Phys. Chem. Chem. Phys.*, 2006, **8**, 5350.
30 L. Wang, T. Maxisch and G. Ceder, Oxidation energies of transition metal oxides within the GGA + U framework, *Phys. Rev. B: Condens. Matter Mater. Phys.*, 2006, **73**(19), 195107.
31 Y. Maimaiti, M. Nolan and S. D. Elliott, Reduction Mechanisms of the CuO (111) Surface through Surface Oxygen Vacancy Formation and Hydrogen Adsorption, *Phys. Chem. Chem. Phys.*, 2014, **16**(7), 3036–3046.
32 P. E. Blöchl; J. Kästner and C. J. Först, Electronic Structure Methods: Augmented Waves, Pseudopotentials and The Projector Augmented Wave Method, *Handbook of Materials Modeling*, 2005, pp. 93–119.
33 G. Kresse and D. Joubert, From Ultrasoft Pseudopotentials to the Projector Augmented-Wave Method, *Phys. Rev. B: Condens. Matter Mater. Phys.*, 1999, **59**, 1758.
34 A. K. Mishra, A. Roldan and N. H. de Leeuw, CuO Surfaces and CO2 Activation: A Dispersion-Corrected DFT+U Study, *J. Phys. Chem. C*, 2016, **120**(4), 2198–2214.
35 J. Hu, D. Li, J. G. Lu and R. Wu, Effects on Electronic Properties of Molecule Adsorption on CuO Surfaces and Nanowires, *J. Phys. Chem. C*, 2010, **114**, 17120–17126.
36 G. Wulff, Zur Frage der Geschwindigkeit des Wachstums und der Auflösung der Kristallflächen, *Z. Kristallogr. - Cryst. Mater*, 1901, **34**, 449–530.
37 M. W. Chase Jr., NIST-JANAF Themochemical Tables, Fourth Edition, *J. Phys. Chem. Ref. Data, Monograph*, 1998, **9**, 1–1951.
38 J. D. Cox; D. D. Wagman and V. A. Medvedev, *CODATA Key Values for Thermodynamics*, Hemisphere Publishing Corp, 1984, p. 1.
39 Standard Thermodynamic Properties of Chemical Substances, ed D. R. Lide, *In CRC Handbook of Chemistry and Physics*, 2010, Vol. 90, pp 4–5.